Author(s): Sharma, Vipul; Parihar, Vijay Singh; Ali-Löytty, Harri; Vihinen, Jorma; Ukale, Dattatraya; Yiannacou, Kyriacos; Lahtonen, Kimmo; Kellomäki, Minna; Sariola, Veikko

Title: Fractal-like Hierarchical CuO Nano/Microstructures for Large-Surface-to-Volume-Ratio Dip Catalysts

Year: 2022

Version: Published version

Please cite the original version:

Fractal-like Hierarchical CuO Nano/Microstructures for Large-Surface-to-Volume-Ratio Dip Catalysts

Vipul Sharma,*,# Vijay Singh Parihar,# Harri Ali-Löytty, Jorma Vihinen, Dattatraya Ukale, Kyriacos Yiannacou, Kimmo Lahtonen, Minna Kellomäki, and Veikko Sariola*

Read Online

ACCESS | Metrics & More | Article Recommendations | Supporting Information

ABSTRACT: Dip catalysts are attracting interest in both academia and industry for catalyzing important chemical reactions. These provide excellent stability, better recoverability, recyclability, and easy scale-up. Using the unique micro-structures of leaf skeletons, we present a fractal-like hierarchical surface that can be used as a versatile and efficient dip catalyst. Copper oxide microcactuses with nanoscalar features were fabricated onto the *Bauhinia racemosa* leaf skeletons via a combination of physical vapor deposition, electroplating, and chemical oxidation methods. The coated leaf skeletons have a very high surface area, and the three-dimensional (3D) morphology allows the reactants to encounter the catalytic sites efficiently and move around the reaction mixture swiftly. The fabricated bioinspired leaf skeleton-based dip catalyst was characterized and demonstrated to be very efficient for alcohol dehydrogenation reaction, examined under different experimental conditions. A ceramic 3D-printed catalyst holder was designed to hold the catalysts to avoid any damage caused by the magnetic bars during the reactions. The performance is determined using the reaction yields, and the efficiencies are correlated with microcactus-like structures composed of CuO and the 3D fractal-like shape provided by the leaf skeleton. This strategy can be applied to fabricate other dip catalysts using different materials and designs, suitable for catalyzing numerous other chemical reactions.

KEYWORDS: copper oxide, leaf skeleton, dip catalyst, bioinspiration, alcohol dehydrogenation
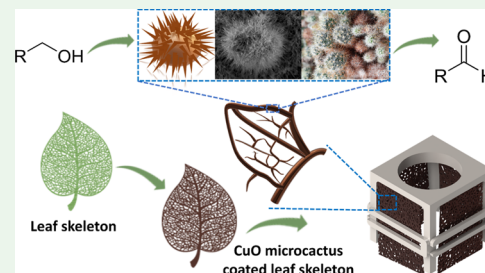
INTRODUCTION

Recently, heterogeneous catalysts are drawing huge attention due to their versatile uses including energy generation,[1] environmental remediation, and synthesis of high-value industrial products.[2,3] To increase their recyclability and efficiency, catalyst nanoparticles have been put onto a film or mounted on a substrate and used as a dip catalyst.[4,5] These types of catalysts are growing in popularity due to their good recyclability, spontaneous reaction manipulation/control, and good turnover number and turnover frequency.[4] Traditionally, the dip catalysts are fabricated in two ways: by assembling the catalytically active material as thin films[4,6] or by immobilizing the catalyst nanoparticles onto a substrate.[7,8] Many methods have been reported in the past to fabricate efficient dip catalysts.[9] The substrates range from sintered inorganic surfaces to biopolymer-based surfaces to immobilize the catalytic nanoparticles. Bioinspired dip catalysts have also been reported where bioinspired surfaces were fabricated to immobilize and lock the catalyst particles to obtain dip catalysts.[10,11] Most commonly, dip catalysts have been demonstrated in Suzuki−Miyaura cross-coupling reactions. However, dip catalysts have also found their applications in catalyzing the degradation of nitroarene compounds,[7] surface-enhanced Raman spectroscopy (SERS) substrates,[5] and sensor substrates.[12] Despite the good efficiency, recyclability, and

versatility, the most common problems in the dip catalysts are related to the lack of surface area (micro/nanostructured morphology), catalyst leaching, surface fouling, and the aggregation of the catalyst particles. Also, the surfaces are often two-dimensional, which restricts the movement of the reactants smoothly during the reaction process.

Copper oxides are very promising catalyst candidates in heterogeneous catalysis because of their extremely low cost, accessibility, and low toxicity as compared to other transition metal oxides.[13,14] Most important use of the CuO catalyst is in the formation of C−S bonds in high-value products that are of medicinal and material interest.[15,16] In addition, CuO particles have also been used in the oxidative dehydrogenation of various primary and secondary alcohols to carbonyl compounds, which is a fundamental reaction in nature and synthetic organic chemistry.[17,18] These reactions are carried out at high temperatures (>200 °C) and need stoichiometric amounts of catalysts, and their scale-up makes the waste
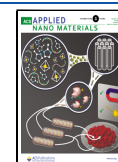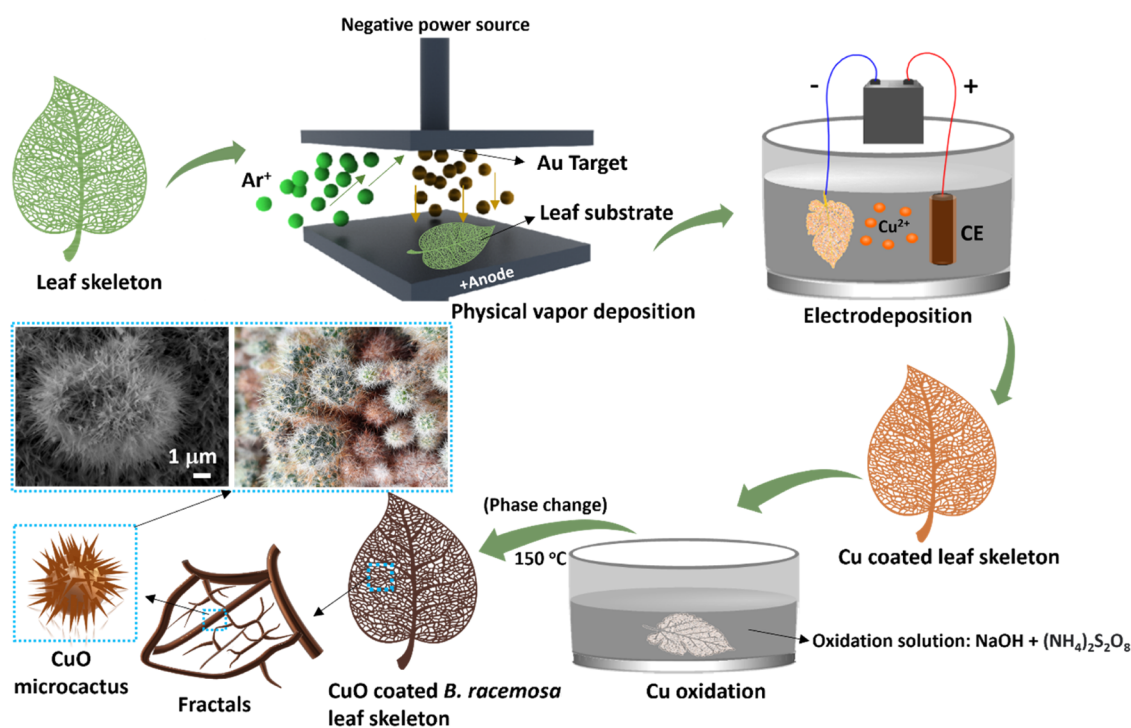
Figure 1. Schematics of the fabrication procedure of CuO microcactus on *B. racemosa* leaf skeleton and dip catalyst assembly.

disposal problematic. Therefore, recent attention is focused on the development of micro/nanostructured CuO-based heterogeneous catalytic surfaces to decrease the impact of these processes on the environment. One of the most popular approaches to preparing the catalytically active micro-/nanostructured CuO is the hydrothermal method.[19−21] This method enables control over the crystallographic structure and in the orientations of the catalytically active sites. Some other wet chemical approaches were also reported to prepare the catalytically active and stable CuO micro/nanostructures.[22−26] In the traditional methods, high temperature, high pressure, and long reaction time are the possible disadvantages as it increases the production cost and scale-up is difficult. Subsequently, it is still worth developing new and effective synthetic methods for high-performance CuO-based catalysts.

Introducing micro/nanoscale roughness and three-dimensional (3D) morphology to the dip catalysts can be challenging. However, the bioinspired surfaces provide well-defined morphological features ranging from macroscale to micro/nanoscale.[11,27−30] These well-ordered microstructures can be found in the eyes of insects,[31] in butterfly wings,[32] gecko feet,[33] various types of leaves,[10,34−36] fish scales,[37] etc. The interplay of the unique multiscale surface morphologies of biological surfaces and the material functions leads to interesting properties. This has encouraged scientists to tailor the surface morphologies to achieve specific functionalities.[37,38] The most important functionality imparted by a fractal-like bioinspired architecture is the high surface-area-to-volume ratio. The high surface area and the organized orientation of the micro/nanostructures enable these functional surfaces to be used in many applications such as water harvesting, self-cleaning surfaces, electronics, etc.[39] The high surface area of the natural surfaces makes them suitable to be utilized in catalysis.[10,11] However, the reports on the biotic and biomimetic surfaces that can be used in the catalysis applications are still very limited, and the only reports include

the immobilization of the already prepared catalyst nanoparticles on the bioinspired surfaces.

In this work, we report a biotic 3D dip catalyst based on leaf skeletons. Leaf skeletons have multiscale interconnected fractal-like structures that display a micromesh-like morphology. The fractal-based design is also beneficial in catalysis because this overcomes the restrictions of the mostly used planar designs by significantly increasing the surface area at the microscale and maximizing the surface-to-volume ratio, using principles of simple scaling. The 3D mesh/fractal-like morphology allows the smooth circulation of the reactants while allowing the maximum catalyst area/catalytic sites to participate in the reaction. Micro/nanostructures with needle-like protrusions were grown on the leaf skeletons using a combination of sputtering, electrodeposition, and chemical oxidation techniques. We call these microstructures "microcactuses" due to their uncanny resemblance to the Texas nipple cactus (*Mammillaria prolifera*). These microstructures increase the overall surface area and the number of catalytically active sites. The properties of the fabricated surfaces are studied using scanning electron microscopy (SEM), energy-dispersive X-ray spectroscopy (EDS) mapping, X-ray diffraction (XRD) analysis, and X-ray photoelectron spectroscopy (XPS). We further demonstrate that the bioinspired dip catalyst is a highly efficient heterogeneous catalyst. The catalytic activity and the versatility of the catalyst are demonstrated in the oxidation of alcohols under mild reaction conditions using atmospheric oxygen as an oxidant. The insights gained from this work will help to repurpose the biotic and nanostructured catalysts as inexpensive, high-surface-area surfaces for catalysis.

■ RESULTS AND DISCUSSION

The fabrication of CuO microcactus on the leaf skeletons of *B. racemosa* plant is shown in Figure 1. Herein, a modified electrodeposition and chemical oxidation process was
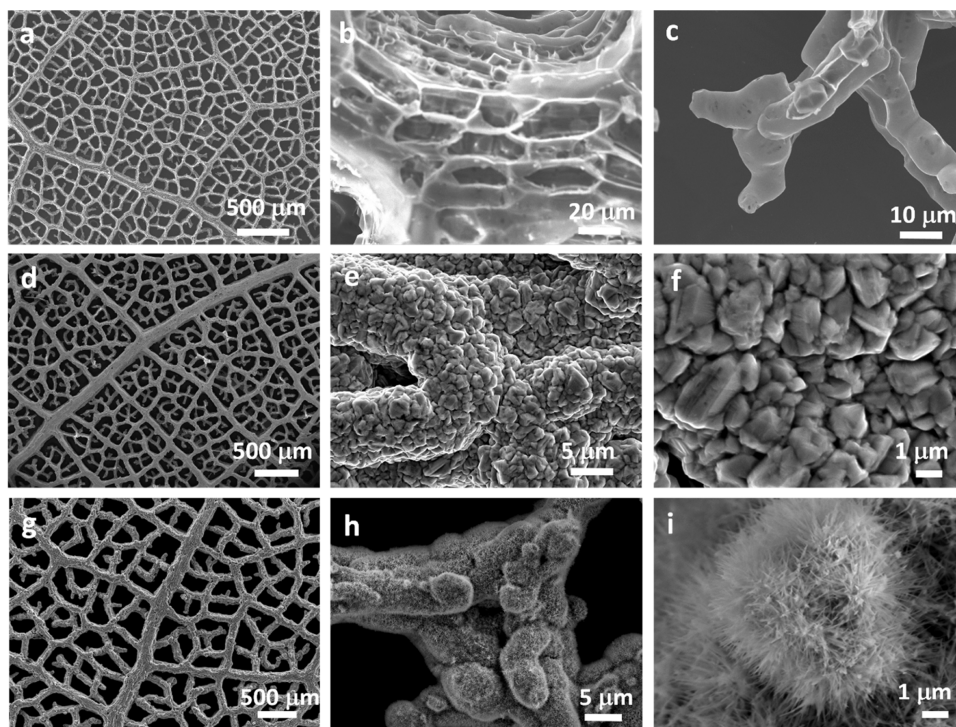
Figure 2. SEM images of the *B. racemosa* leaf skeleton with Au coating (a−c), Cu coating after electrodeposition (d−f), and CuO microcactus (g−i) at different resolutions.

combined that helps in the three-dimensional uniform coating of the leaf skeleton with CuO.

Generally, there is a significant variation in the size, vein orientation, area coverage, fractal dimensions, and topographies between the leaf skeletons of different plant species.[40,41] In this work, leaves of *B. racemosa* were chosen due to their commercial availability, high surface area,[42] and interesting fractal structures. Figure 2 displays the SEM images of the leaf skeletons before the electrodeposition, after Cu deposition, and after oxidation. The microcactuses form from electrodeposited Cu film during the chemical oxidation process. Figure 1 shows the schematics and camera images (insets) of the preparation procedure. We have demonstrated the mechanism of the formation of similar CuO structures at the surface of the copper during the oxidation process in our previous reports.[43] The CuO particles that etch off from the surface of the leaf skeleton have high surface energies and are very reactive as well. Due to the 3D surface and unique morphology provided by the leaf skeleton of *B. racemosa*, the CuO particles aggregate around the rough micro blocks created during the Cu deposition process (Figure 2e,f). As evidenced from the figure, these micro blocks usually range from 1 to 3 μm in diameter. The oxidation of Cu to CuO leads to the nanoneedle-like structures on these micro blocks and makes the structures look like microcactus. The microcactus-based surface displayed a very good surface area of 3.09 ± 0.03 m^2 g^{-1}, which was calculated using the Brunauer−Emmett−Teller (BET) surface area method (refer Figure S1, Supporting Information). This surface area may not be comparable to the noble metal nanoparticle-based catalyst dispersed in a solution but is high compared to other reported CuO nanoparticles, commercial bulk CuO, and other heterogeneous dip catalysts.[44−46]

Control samples with planar surfaces were also fabricated. A CuO layer was grown on copper plates following the same procedure as above. We noticed random nanograss-like structures (Figure S2, Supporting Information) that are due to the lack of micro-block-like structures and the 3D orientation provided by the leaf skeleton. It should be noted that leaf skeletons of different plant species have different morphologies on the micro- and macroscale, and the use of different leaf skeletons affects the deposition of Cu and eventually leads to the change in the CuO microstructure morphology. In addition, a modified chemical oxidation process leads to the different shapes of the CuO microstructures that we have demonstrated in our previous studies.[43,47]

SEM was employed to characterize surface microstructures, and the images at different resolutions are displayed in Figure 2. In Figure 2a−c, the Au-coated leaf skeleton of *B. racemosa* can be seen, and the internal vascular bundles along with lignin fibers are also clear. It is noteworthy to mention that a thin Au layer does not affect the morphology of the microstructures present in the fractals and is a common practice to make surfaces conducting before SEM measurements. Their arrangement gives the dense fractal-like geometry at the milli- and microscales. Unlike the other leaf skeletons reported in the literature,[41,48,49] the leaf skeletons are denser and the average gap between the fractals ranges from 10 to 20 μm. Figure 2d−f shows the *B. racemosa* leaf skeleton after Cu electrodeposition. As evidenced from the images, Cu has been deposited uniformly along the skeleton surfaces. The Cu is deposited in the form of 3D micro blocks/slabs having an average diameter of ∼500 nm to 2 μm. This is due to the irregular and unique surface of the *B. racemosa* leaf skeleton. It is noteworthy to mention that the type of the skeleton and the surface morphology may lead to variations in the electrodeposited
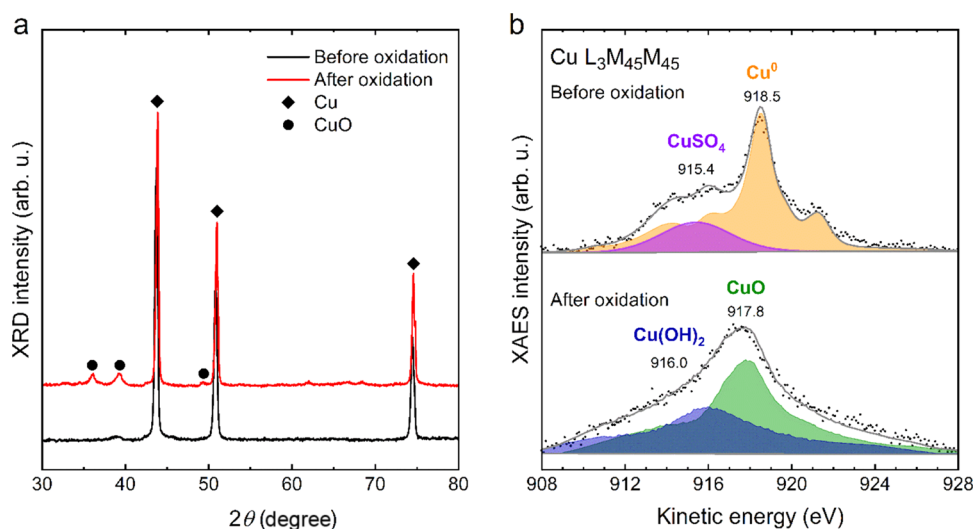
Figure 3. (a) XRD pattern of Cu-coated leaf skeletons before and after oxidation. (b) High-resolution XPS core-level spectra of (a) Cu and (b) CuO. CuO and Cu(OH)$_2$ were fitted using experimental references, and CuSO$_4$ is fitted using a synthetic component.
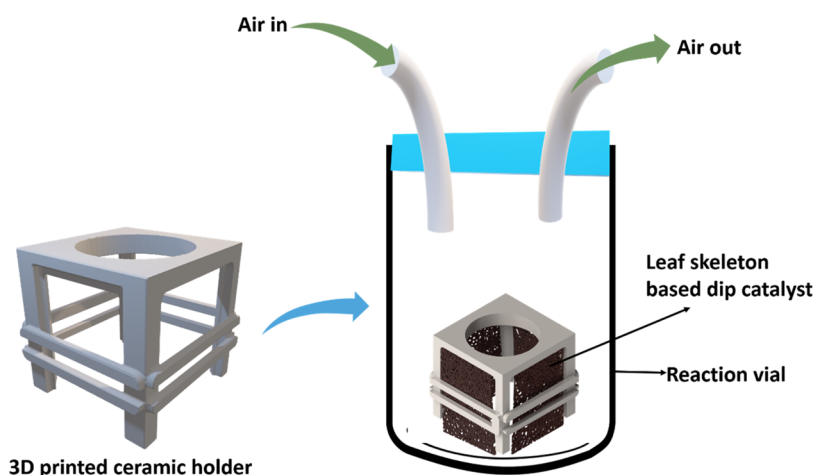
Figure 4. Preparation of ceramic 3D-printed dip catalyst holder and reaction setup.

metal coatings.[43,50] Figure 2g–i shows the CuO microcactus structures bearing nanoneedles formed after the oxidation process. The structures display an average diameter in the range of 2–20 μm and have dense nanoneedles arranged in 3D that make the morphology look like a microcactus. It is also clear from the SEM images that the dense fractal-like morphology was intact after the fabrication process and the CuO microcactus cover the whole surface. EDS was used to confirm the presence of Cu on the leaf skeleton surfaces. The EDS data confirm the presence of Cu and CuO on the leaf skeleton surfaces and are shown in Figures S3 and S4, Supporting Information.

The phase purity and structural characteristics of the Cu and CuO microcactus on the leaf skeletons were conducted using XRD analysis shown in Figure 3a. The XRD peaks in CuO microcactus appeared at 2θ (36, 39.3, 43.8, 49.4, 51, 61.9, 66.7, 68.4, 74.6°) values. Here, the peaks at 36, 39.3, 49.4, 61.9, 66.7, and 68.4° can be assigned to the (002), (111), (202), ($\bar{1}$13), (311), and (220) planes that originate from CuO crystalline phases (JCPDS card no. 45-0937), while the peaks at 43.8, 51, and 74.6° come from the (111), (200), and (220) planes from the copper film underneath (JCPDS card no. 85-1326). Before oxidation, only peaks of metallic copper were present. The

presence of metallic peaks after the oxidation indicates that only the surface of metallic Cu has transformed to CuO in the oxidation treatment. The XRD spectra show that the CuO microcactuses are crystalline with the monoclinic structure, which corresponds to the CuO.[51] The other crystalline phases of copper oxide such as Cu(OH)$_2$ and Cu$_2$O were not observed.[52] The XRD results show that the CuO micro-cactuses fabricated on the leaf skeletons grow in a single phase and have a high degree of purity. XRD also confirmed the presence of CuO on the surfaces.

XPS was used to analyze the chemical composition of the sample surfaces. The chemical state of Cu was analyzed from the Cu LMM Auger transition shown in Figure 3b since it is more sensitive to different chemical states than the Cu 2p core-level peak. Before chemical oxidation treatment, that is after electroplating, the surface consisted of primarily metallic Cu (Cu^0) with some CuSO$_4$.[53] The composition is typical for an electroplated Cu surface containing some traces of CuSO$_4$ plating solution. After the chemical oxidation treatment, the surface had oxidized to Cu^{2+}−O and Cu^{2+}−(OH)$_2$. The presence of metastable hydroxylated Cu^{2+} is characteristic of the chemical oxidation, was detected only for freshly treated samples, and is subject to transform to a more stable CuO

(Figure S5).[54] Therefore, the chemical state of the micro-cactuses was identified as CuO.

The application of the dip catalyst was demonstrated using alcohol dehydrogenation reactions. A ceramic 3D-printed catalyst holder was used to hold the catalysts to avoid any damage caused by the magnetic bars during the reactions, as shown in Figure 4. The general scheme of the alcohol dehydrogenation reactions is shown in Scheme 1. Although

Scheme 1. General Schematic of the Alcohol Dehydrogenation Reactions Using a Dip Catalyst

$$R\diagup OH \xrightarrow[\text{toluene, 100 °C, 24 hr}]{\text{CuO, microcactus}} R-C(=O)H$$
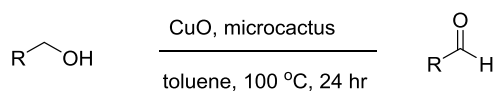
various forms of copper oxide can catalyze the alcohol dehydrogenation reaction, only copper in the oxidation state +2 is reported to show significant activity and good selectivity for the oxidation of alcohols.[55,56] For the model reaction, the oxidation of benzyl alcohol was investigated in the presence of CuO microcactus-coated leaf skeleton as a dip catalyst. The reaction was carried out in toluene at 100 °C and air (1 atm pressure). The reaction was swift and gave an excellent yield for the aldehyde as the product. The bioinspired dip catalyst displayed very good selectivity of >80 and ~90% conversion efficiency. There was no sign of disproportion products such as esters, acids, alcohols, etc., which indicated that there was no overoxidation during the reaction as evident from the corresponding NMR spectra and high-performance liquid chromatography (HPLC) spectra (refer to the Supporting Information). The planar surface consisting of CuO grown on a glass slide was used as a control. Although the control surfaces were able to catalyze the alcohol dehydrogenation reaction, the yield was low (55%) as compared to the bioinspired dip catalyst. This may be due to the low surface area of the control due to their planar structure as compared to the skeleton samples as suggested by the BET analysis. The yield of the reaction with the control sample will be increased when some extra CuO-decorated plates will be inserted. A control experiment without any catalyst was also performed, and the benzaldehyde formation was very minimal under the specified reaction settings.

To optimize the best reaction conditions, the bioinspired dip catalyst was tested in atmospheric air at different temperatures. It is clear from Table 1 that on increasing the reaction

Table 1. Influence of Temperature on the Activity and Leaching of CuO Microcactus toward the Oxidation of Benzyl Alcohol to Benzaldehyde[a,b]

s. no.	temperature (°C)	conversion (%)	selectivity	yield	leaching (ppm Cu)
1	room temperature	~5	>90	~4	0.0
2	40	~15	>95	~14	2.9
3	60	~18	>95	~19	1.2
4	80	~61	>95	~64	5.4
5	100	>95	>95	>95	5.4

[a]The amount of leached Cu during the test was normalized to the mass of Cu catalyst (108 mg) in the test. [b]Reaction conditions: benzyl alcohol (4.62 mmol), toluene (dry, 30 mL), catalyst (3 × 2 cm × 2 cm strips, 10 μm equiv thickness of Cu), 24 h, atmospheric oxygen.

temperatures (R.T.−100 °C), the conversion percentage of the benzyl alcohol to benzaldehyde increases significantly. The bioinspired dip catalyst displayed more selectivity for benzaldehyde at higher temperatures, and the variation in selectivity increased from ~90 to ~98% within 24 h. It is noteworthy to mention that the catalyst amount is directly linked to the rate and the efficiency of the reactions. Hence, in this case, a multilevel catalyst holder can accommodate even more catalyst strips that may lead to higher yields.

Figure 5 shows the time-dependent catalytic performance of the bioinspired dip catalyst and the control planar surfaces. It is
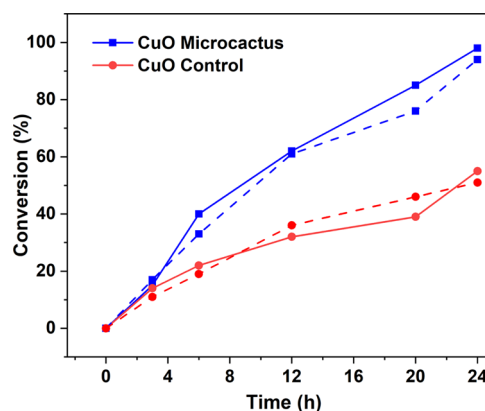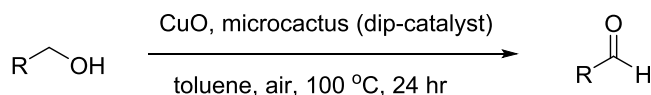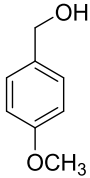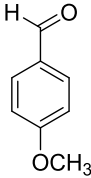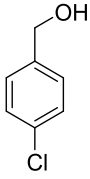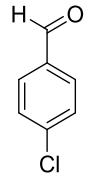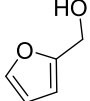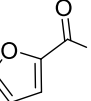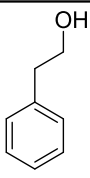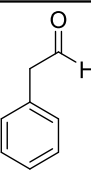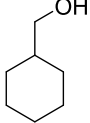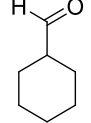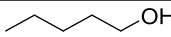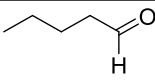

Figure 5. Time-dependent oxidation of benzyl alcohol over CuO microcactus and the control sample. Reaction conditions: benzyl alcohol (4.62 mmol), toluene (dry, 30 mL), catalyst (3 strips), 24 h, 100 °C, atmospheric air. The solid lines show the yields calculated using HPLC, and the dashed lines correspond to the isolated yields.

clear from the figure that the initial rate of the reaction is low, and the reaction kinetics was almost similar for both samples, indicating the initial induction period. After around 8 h, the conversion of the benzyl alcohol to the benzaldehyde reached only ~15% for both the bioinspired dip catalyst and the control samples. But after 24 h, the reaction mixture having bioinspired dip catalyst had >95% yield, while the control samples only gave ~55%. The induction period originates due to the slow temperature rise of the reaction mixture to the target temperature, low surface−substrate interaction, and the catalyst wetting process.

Once the reaction conditions were optimized, the bioinspired dip catalyst was employed to check the scope of aldehyde formation with available alcohols. To demonstrate the versatility of the catalyst, aromatic alcohols having electron-withdrawing and -donating groups were used, as seen in Table 2. From the table, it can be seen that the catalyst was able to catalyze the conversion of a variety of alcohols with very good selectivity. To prove the diversity of the dip catalyst, we selected the substrates with different groups (−R) attached to the reactive hydroxyl group. For the model reaction to optimize the reaction conditions with benzyl alcohol and then substituted benzyl alcohol, i.e., 4-methoxybenzyl alcohol (a group with +R effect, entry 1) 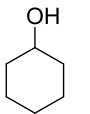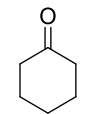and 4-chlorobenzyl alcohol (a group with -I effect, entry 2), we further expand the diversity of the dip catalyst we have chosen, heterocyclic alcohol (entry 3), unsaturated cyclic (entries 5 and 6), and noncyclic alcohols (entry 7, Table 2). In general, the oxidation reaction yields for aromatic and heterocyclic alcohols are higher than the unsaturated alcohols due to the stability of the reactive intermediate (Cu−alcohol complex) as shown in the reaction

Table 2. Percentage Yield of Alcohol Dehydrogenation Reaction of Various Alcohols Using a Bioinspired Dip Catalyst in the Presence of Atmospheric Air[a]

$$\text{R}\diagup\text{OH} \xrightarrow[\text{toluene, air, 100 °C, 24 hr}]{\text{CuO, microcactus (dip-catalyst)}} \text{R}\diagup\text{C(=O)H}$$

Entry	Alcohol	Aldehyde	% Yield (isolated)
1	4-methoxybenzyl alcohol (OCH₃ para, CH₂OH)	4-methoxybenzaldehyde (OCH₃ para, CHO)	92 ± 4
2	4-chlorobenzyl alcohol (Cl para, CH₂OH)	4-chlorobenzaldehyde (Cl para, CHO)	90 ± 3
3	furfuryl alcohol	furfural	86 ± 6
4	2-phenylethanol	phenylacetaldehyde	81 ± 6
5	cyclohexylmethanol	cyclohexanecarbaldehyde	84 ± 3
6	cyclohexanol	cyclohexanone	89 ± 2
7	pentan-1-ol	pentanal	81 ± 4

[a]Reaction conditions: alcohol (500 mg), toluene (dry, 30 mL), catalyst (3 strips), 24 h, 100 °C, atmospheric air.

mechanism. We anticipate that the reactive carbon in the Cu–reactant complex is electron-deficient; hence, the aromatic groups and electron-donating groups will increase the stability of the complex, and this stabilization mechanism increases the reaction yields. On the contrary, reactive centers that attach to the electron-withdrawing or unsaturated groups reduce the stability and eventually lead to lower yields.

One of the major advantages of the dip catalyst is its recycling capability. An additional important benefit of biotic dip catalysts demonstrated in this study is the ease with which the catalyst can be monitored throughout the recyclability runs, and it is not easy with most of the reported procedures for the catalyst immobilization.[57,58] The recyclability of the catalysts in the dehydrogenation reactions was tested using the

dehydrogenation of benzyl alcohol as the base reaction. In the first run, a yield of ~98% was reported. For the recyclability experiments, the dip catalyst was taken out after each cycle, washed, dried at room temperature, and reused for the next reaction cycle. In this case, it was found that the catalysts were reusable, and the yields obtained after six cycles were very good with an average fluctuation of ~5% in each cycle, as seen in Figure 6. Negligible wearing or leaching of the CuO was
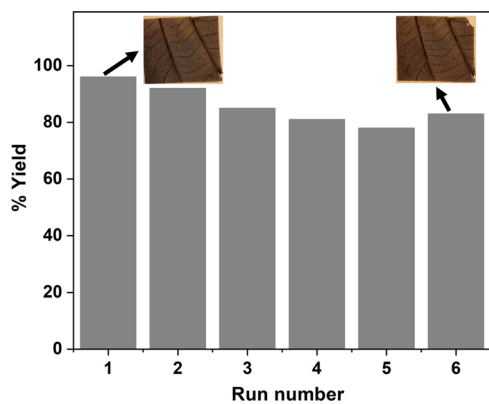
Figure 6. Percentage yields obtained in repetitive runs of the alcohol dehydrogenation reaction using CuO microcactuses on leaf skeleton-based dip catalysts. Reaction conditions: benzyl alcohol (4.62 mmol), toluene (dry, 30 mL), catalyst (3 strips), 24 h, atmospheric oxygen.

observed from the surface and was confirmed by the inductively coupled plasma mass spectrometry (ICP-MS) (refer to Table 1). We observed that the nanoneedles seem to be settled in this case after the reaction; however, the surface roughness was still very high (refer to Figure S5, Supporting Information). The oxidation state of the copper oxide was also

maintained after the first run as confirmed by XPS (Figure S6, Supporting Information). The planar control samples had a significant loss in the catalytic activity with the yields dropping to less than 50% after the first run and less than 15% in the second run. This suggests that the catalytic activity of the control sample might be because of the leaching of the material from the surface of the film. In the general heterogeneous catalyst system, turnover numbers are used for the estimation of the longevity of a catalyst system and turnover frequency shows the kinetics of a reaction. This requires the estimation of the active catalytic sites, which is usually possible in a nanoparticle-based system, and the values can be calculated theoretically and practically. Also, this makes more sense when precious metals like Pd or Pt are used for the catalytic processes. However, in the current system, it is very difficult to exactly predict or calculate how much of the Cu is converted to copper oxide; hence, the exact estimation of the catalytic sites is not possible.

A brief mechanism for CuO microcactus-catalyzed alcohol dehydrogenation under aerobic conditions is shown in Figure 7, where the dehydrogenation of benzyl alcohol to benzaldehyde is taken as a model reaction. In a typical reaction cycle, benzyl alcohol adsorbs on the rough CuO microneedles and active microscopic catalytic sites, creating a Cu−alkoxide intermediate. The deprotonation is facilitated by the neighboring surface oxygen. This is followed by Cu(II)-induced β-H elimination, which generates Cu(II) hydride and a benzyl carbocation. This intermediate eventually leads to the aldehyde formation. Finally, the oxygen interacts with the hydride to form a peroxide anion and regenerates the catalytic Cu(II) site. After this step, the peroxide anion reacts with a second hydride to further reduce it to hydroxide anions, which further react to produce water as the only side product. Poreddy et al. have recently suggested that redox cycling of
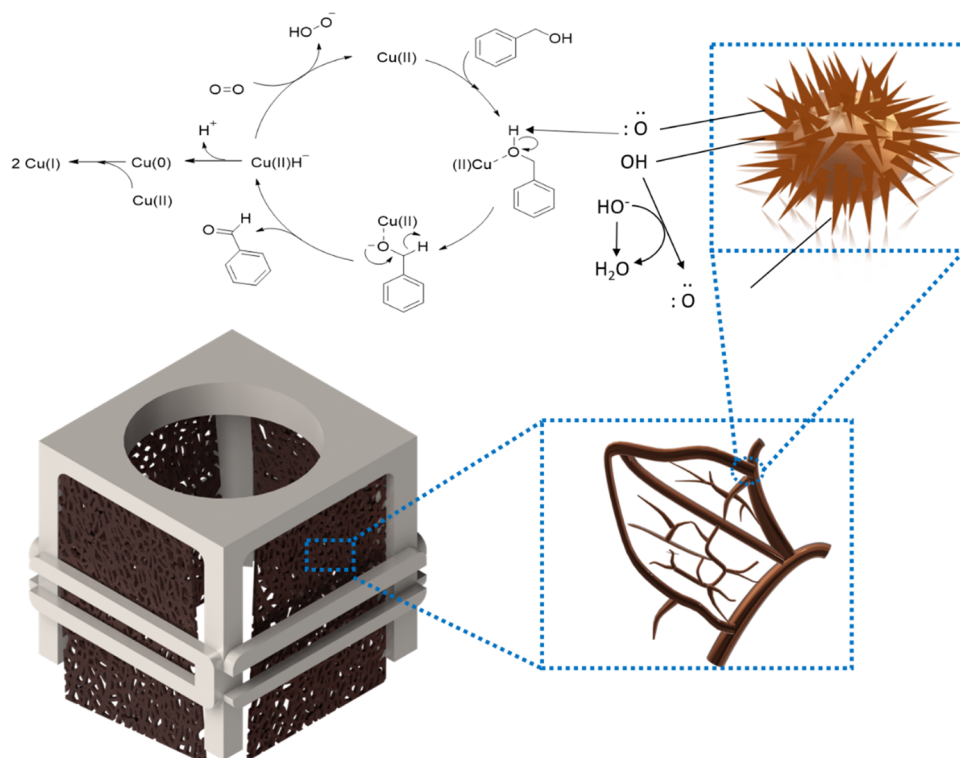
Figure 7. Mechanism schematic of the CuO microcactus-catalyzed alcohol dehydrogenation reaction.

active copper centers is involved in a similar mechanism involving the use of CuO for alcohol dehydrogenization.[18] The high surface area provided by the Cu microcactus acts as the microcavities. These cavities act as microreactors and facilitate the interaction of the reactants with the catalysts efficiently toward product formation.

Overall, the results reveal that electrodeposition and chemical oxidation are effective tools to grow the high-surface-area CuO on the surfaces. The surface features of the leaf skeleton play a crucial role in manipulating the morphology of the CuO. As compared to the control samples with a planar surface, the biotic dip catalysts based on leaf skeletons offer microtextured structures in the form of microcactuses, which allow the reactants to move freely and interact with the catalyst. Herein, the cavities created by the nano and microstructures act as microreactors for catalysis in addition to offering multiple catalytic sites, as demonstrated in this case for the oxidative dehydrogenation of the alcohols. The catalysts were even better suited as catalysts for the oxidative dehydrogenation of the alcohols. Very good recyclability was observed with minimal stripping and leaching of the catalyst. The control surfaces have micrograss-like structures arranged in 2D that limit the availability of the catalytically active surfaces and limit the catalytic activity. Most of the materials used in the fabrication of biotic dip catalysts are inexpensive and come from a sustainable source. For the proof of concept, a very thin film of Au was used as the preliminary conductive layer for electrodeposition, which is expensive. However, for large-scale applications, a thin layer of other inexpensive metals can also be deposited to make the overall process more cost-effective. The insights from this study will help to design efficient catalytic systems where bioinspired designs can be combined with a variety of catalytic materials using different deposition techniques.

CONCLUSIONS

In conclusion, we propose a new method of producing high-surface-area microcactus-like morphology onto the leaf skeletons having a high surface area to obtain an efficient dip catalyst. First, copper oxide microtufts resembling the *M. prolifera* were fabricated onto the *B. racemosa* leaf skeletons using a combination of physical vapor deposition, electrodeposition, and chemical oxidation. The fabricated surfaces with microcactus-like morphology displayed high surface area and a freestanding surface. The biotic dip catalysts were productively used in large-scale oxidative alcohol dehydrogenation reactions. A 3D-printed ceramic catalyst holder was designed and fabricated to hold the catalyst strips so that the catalytic reaction can proceed swiftly. The leaf skeletons bearing CuO microtufts provided very good yields along with good recycling capabilities and easy redeployment during each reuse cycle. The bioinspired dip catalyst system was very versatile and was able to catalyze the dehydrogenation of various types of alcohols with high yields. Based on our study, it can be concluded that the unique shape of the CuO microcactus and the fractal structures of the leaf skeleton determine the performance of the biotic dip catalysts. The CuO and leaf skeleton-based dip catalysts with easy fabrication, convenient handling, easy deployment, commercial viability, and recyclability, complemented with good catalytic efficiency can prove very useful in catalyzing many other synthetic organic reactions as well. This method demonstrated here can be easily applied to a large scale as well and makes it suitable for industrial use.

EXPERIMENTAL SECTION

Materials. Toluene, 99.85% extra dry over a molecular sieve (ACROS Organics), was used as a reaction solvent. Ethyl acetate, 99.9%, and petroleum ether (boiling range 40−60) used for column purification were procured from VWR. Thin-layer chromatography (TLC) plates used to monitor the reaction progress were obtained from Sigma-Aldrich (silica gel on aluminum foils with fluorescent indicator 254 nm). Silica gel used for column chromatography was procured from Sigma-Aldrich (high-purity grade, pore size 60 Å, 70−230 mesh, 63−200 μm). Leaf skeletons of *B. racemosa* were supplied by "Leaf Vein Crafts", Toronto, Canada.

Electrodeposition of the Cu onto the Leaf Skeleton. Leave skeletons of *B. racemosa* were cut into equal dimensions, and a Au layer (~30 nm) was first sputtered onto the surfaces to provide sufficient conductivity for electrodeposition. Then, the Au-coated leaf skeletons were electrodeposited with Cu from an acidic plating solution consisting of 1 M H_2SO_4 (95−97% H_2SO_4, 1.00731.1011 Merck Emsure, Merck), 0.5 M $CuSO_4$ ($CuSO_4 \cdot 5H_2O$, 209198-500G copper(II) sulfate pentahydrate, ACS reagent, ≥98.0%, Sigma-Aldrich), 1 μM HCl (37% HCl, H 396 Romil-SpA Super Purity Acid, Romil), and ultrapure deionized H_2O (18.2 MΩ cm, Merck Milli-Q). The electrodeposition was made in a 1 L polypropylene beaker using a power source (Thurlby Thandar TSX3510 DC Power Supply). The leaf skeleton served as the cathode, and a copper foil (99.99%) was used as the anode. The connections to the electrodes were made using Cu alligator clips. A stativ was used to support all of the electrodes in the cell. The electrodeposition was performed using a galvanostatic method at −10 mA cm^{-2} at room temperature. The electrodeposition time was 45 min 21 s that corresponds to 10 μm cm^{-2} Cu film thickness on a planar surface. A sufficiently thick Cu coating was required to provide the dip catalyst with adequate mechanical strength. For simplicity, the surface area of a leaf skeleton was approximated as the surface area of an intact leaf. We note that the actual surface area of a leaf skeleton and the Cu film thickness is different. However, the method allowed high reproducibility of similar Cu coatings on different-sized leaves. After the electrodeposition, the sample was gently washed with deionized H_2O and dried with a mild stream of N_2.

Fabrication of CuO Microcactus on the Leaf Skeleton Surfaces. To convert the surface of the Cu leaf skeleton to CuO microcactuses, we used a chemical oxidation method described previously.[43] The Cu-deposited leaf skeletons were first gently rinsed with ethanol and deionized H_2O (ELGA PURELAB Option-R7) and ultrasonicated for 15 min in each. The surfaces were then blown-dried with N_2. The Cu-coated leaf skeletons were then transferred to a container with an aqueous solution of 1 wt % NaOH and $(NH_4)_2S_2O_8$ (1:1). The sample containing the solution was then gently stirred at room temperature for 15 min. The samples were then taken out and rinsed with ethanol followed by deionized water. The samples were put in an oven at 150 °C for 2 h to allow the phase change from hydroxide (bluish brown) to oxide (dark brown).

Preparation of the Ceramic Catalyst Holder for the Reaction. The catalyst holder was 3D-printed using a Lithoz CeraFab 7500 ceramic 3D printer. A commercial alumina slurry LithaLox HP 500 was used to avoid it potentially interfering with the chemical reactions. For the reactions, catalysts of area 2 cm × 2 cm were cut using scissors. The surfaces were then mounted onto the 3D-printed catalyst holder (Figure 4) so that the reactants have access to the catalyst surface without any damage caused by the magnetic bead.

Characterization. The surface morphology was studied using a scanning electron microscope (SEM) operating at 15 kV (JEOL IT-500). The samples were mounted onto an aluminum stub and carbon tape (Agar Scientific). Elemental analysis was conducted using energy-dispersive X-ray spectroscopy (EDS) accessory connected to the SEM. The surface chemical analysis was performed by an X-ray photoelectron spectroscopy (XPS) system equipped with an X-ray

source (Al Kα, 1486.6 eV) and a hemispherical electron spectrometer (VG MicrotechCLAM 4). The binding energy scale was referenced to the C 1s C—C/H peak at 284.8 eV. The chemical state of Cu was analyzed from Cu LMM transition by least-squares fitting of experimental line shapes recorded for Cu^0, Cu_2O, CuO, and $Cu(OH)_2$ references.[59] To prepare $Cu(OH)_2$ reference, a piece of Cu foil (99.99%) was first dissolved in HNO_3. Then, the solution was neutralized with NaOH, which resulted in the precipitation of blue $Cu(OH)_2$ that was dried for XPS analysis. A synthetic Gaussian component was used for $CuSO_4$. X-ray diffraction (XRD) measurements were performed using a PANalytical Empyrean multipurpose X-ray diffractometer using Ni-filtered Cu Kα irradiation ($\lambda = 0.1542$ nm) at 40 kV and 40 mA in 2θ ranging from 5 to 80° with a scan rate of 2° min^{-1} with a stepping size of 0.02°. The Cu catalyst concentration in the solution after the reaction was determined using inductively coupled plasma mass spectrometry (ICP-MS) (Thermo Scientific iCAP RQ). Ionic standard solution with a concentration range of 0.001−1000 μg L^{-1} for Cu was prepared in 2% HNO_3 using super-pure chemicals (Romil-SpA) and applied to measure the calibration curve. The limit for detection of Cu leaching in the catalytic test was 0.06 ppm. Ultrapure H_2O (18.2 MΩ cm, Merck Milli-Q) was used for solution preparations. Toluene samples (0.5 mL) were first evaporated to dryness and then dissolved in 5 mL of 2% HNO_3. The surface area of the CuO microcactus-bearing *B. racemosa* leaf skeletons was determined with a Micromeritics 3Flex adsorption analyzer with nitrogen gas under liquid nitrogen. The crude lyophilized product was purified by RP-HPLC using Thermo Scientific 250 × 10 Hypersil ODS 5 μm, flow rate 3 mL min^{-1} using isocratic elution of CH_3CN and H_2O (50:50, v/v) desired fraction was collected and dried. ^1H and ^{13}C nuclear magnetic resonance (NMR) spectra were recorded on Bruker Avance 400 and 500 NMR spectrometers and a JEOL-500 MHz instrument (SCZ500R, JEOL Resonance, Japan) in CDCl$_3$ as solvent. Chemical shifts (δ, ppm) are cited relative to the residual solvent peak (as an internal standard).

Alcohol Dehydrogenation Experiments. In the general dehydrogenative alcohol oxidation reaction, the three dip catalyst strips (2 cm × 2 cm) were mounted on a 3D ceramic holder, which was gently immersed in a glass reaction vessel in 30 mL of dry toluene. To this reaction assembly, 500 mg of substrate (alcohol) was added and the reaction vessel was sealed and stirred at 100 °C for 24 h. The oxygen inside the reaction vessel at atmospheric pressure acts as an oxidant for the dehydrogenative oxidation of alcohol. After 24 h, the reaction mixture was freeze-dried, and the crude reaction mixture was purified by column chromatography on silica gel with petroleum ether and ethyl acetate solvent system. The isolated yields were reported from the purified products, and the pure aldehydes were characterized by proton and carbon NMR spectroscopy. For the optimization of the model reaction (benzaldehyde), the HPLC was performed for the crude reaction mixture to determine the percentage conversion, and the pure compound was collected from HPLC and characterized by NMR spectroscopy.

ASSOCIATED CONTENT

Supporting Information

The Supporting Information is available free of charge at https://pubs.acs.org/doi/10.1021/acsanm.2c02959.

> BET surface area estimation; SEM images of the control sample; EDS mapping; SEM image of the dip catalyst after dehydrogenation reaction; additional XPS spectra; NMR spectra; and HPLC chromatogram of corresponding products (PDF)

AUTHOR INFORMATION

Corresponding Authors

Vipul Sharma − *Faculty of Medicine and Health Technology, Tampere University, 33720 Tampere, Finland;* orcid.org/0000-0002-4460-4610; Email: vipul.sharma@tuni.fi

Veikko Sariola − *Faculty of Medicine and Health Technology, Tampere University, 33720 Tampere, Finland;* orcid.org/0000-0001-8307-6120; Email: veikko.sariola@tuni.fi

Authors

Vijay Singh Parihar − *Biomaterials and Tissue Engineering Group, BioMediTech, Faculty of Medicine and Health Technology, Tampere University, 33720 Tampere, Finland;* orcid.org/0000-0002-6044-2121

Harri Ali-Löytty − *Surface Science Group, Photonics Laboratory, Tampere University, FI-33014 Tampere, Finland;* orcid.org/0000-0001-8746-7268

Jorma Vihinen − *Faculty of Engineering and Natural Sciences, Tampere University, FI-33014 Tampere, Finland*

Dattatraya Ukale − *Department of Chemistry & Nanoscience Centre, University of Jyväskylä, FI-40014 Jyväskylä, Finland*

Kyriacos Yiannacou − *Faculty of Medicine and Health Technology, Tampere University, 33720 Tampere, Finland;* orcid.org/0000-0001-6270-5733

Kimmo Lahtonen − *Faculty of Engineering and Natural Sciences, Tampere University, FI-33014 Tampere, Finland;* orcid.org/0000-0002-8138-7918

Minna Kellomäki − *Biomaterials and Tissue Engineering Group, BioMediTech, Faculty of Medicine and Health Technology, Tampere University, 33720 Tampere, Finland;* orcid.org/0000-0003-4321-1820

Complete contact information is available at:
https://pubs.acs.org/10.1021/acsanm.2c02959

Author Contributions

[#]V.S. and V.S.P. have contributed equally to the work.

Notes

The authors declare no competing financial interest.

ACKNOWLEDGMENTS

REFERENCES

(1) Wang, J.; Cui, W.; Liu, Q.; Xing, Z.; Asiri, A. M.; Sun, X. Recent Progress in Cobalt-based Heterogeneous Catalysts for Electrochemical Water Splitting. *Adv. Mater.* **2016**, *28*, 215−230.

(2) Jiang, X.; Nie, X.; Guo, X.; Song, C.; Chen, J. G. Recent Advances in Carbon Dioxide Hydrogenation to Methanol via Heterogeneous Catalysis. *Chem. Rev.* **2020**, *120*, 7984−8034.

(3) Bavykina, A.; Kolobov, N.; Khan, I. S.; Bau, J. A.; Ramirez, A.; Gascon, J. Metal−Organic Frameworks in Heterogeneous Catalysis: Recent Progress, New Trends, and Future Perspectives. *Chem. Rev.* **2020**, *120*, 8468−8535.

(4) Hariprasad, E.; Radhakrishnan, T. P. Palladium Nanoparticle-Embedded Polymer Thin Film "Dip Catalyst" for Suzuki−Miyaura Reaction. *ACS Catal.* **2012**, *2*, 1179−1186.

(5) Zheng, G.; Polavarapu, L.; Liz-Marzán, L. M.; Pastoriza-Santos, I.; Pérez-Juste, J. Gold Nanoparticle-Loaded Filter Paper: A Recyclable Dip-Catalyst for Real-Time Reaction Monitoring by

Surface Enhanced Raman Scattering. *Chem. Commun.* **2015**, *51*, 4572−4575.

(6) Rao, V. K.; Radhakrishnan, T. P. In Situ Fabricated Ag/AgCl-Polymer Nanocomposite Thin Film: An Appraisal of the Efficient and Reusable Photocatalyst. *Mater. Res. Bull.* **2017**, *87*, 193−201.

(7) Ahmad, I.; Kamal, T.; Khan, S. B.; Asiri, A. M. An Efficient and Easily Retrievable Dip Catalyst Based on Silver Nanoparticles/ Chitosan-Coated Cellulose Filter Paper. *Cellulose* **2016**, *23*, 3577−3588.

(8) Xiang, Z.; Chen, Y.; Liu, Q.; Lu, F. A Highly Recyclable Dip-Catalyst Produced from Palladium Nanoparticle-Embedded Bacterial Cellulose and Plant Fibers. *Green Chem.* **2018**, *20*, 1085−1094.

(9) Madhuri, U. D.; Saha, J.; Radhakrishnan, T. P. 'Dip Catalysts' Based on Polymer-Metal Nanocomposite Thin Films: Combining Soft-Chemical Fabrication with Efficient Application and Monitoring. *ChemNanoMat* **2018**, *4*, 1191−1201.

(10) Sharma, V.; Kumar, S.; Bahuguna, A.; Gambhir, D.; Sagara, P. S.; Krishnan, V. Plant Leaves as Natural Green Scaffolds for Palladium Catalyzed Suzuki−Miyaura Coupling Reactions. *Bioinspiration Biomimetics* **2017**, *12*, No. 016010.

(11) Sharma, V.; Bahuguna, A.; Krishnan, V. Bioinspired Dip Catalysts for Suzuki-Miyaura Cross-Coupling Reactions: Effect of Scaffold Architecture on the Performance of the Catalyst. *Adv. Mater. Interfaces* **2017**, *4*, No. 1700604.

(12) Balaji, R.; Renganathan, V.; Chen, S.-M.; Singh, V. Ingenious Design and Development of Recyclable 2D BiOCl Nanotiles Attached Tri-Functional Robust Strips for High Performance Selective Electrochemical Sensing, SERS and Heterogenous Dip Catalysis. *Chem. Eng. J.* **2020**, *385*, No. 123974.

(13) Singh, J.; Kaur, G.; Rawat, M. A Brief Review on Synthesis and Characterization of Copper Oxide Nanoparticles and Its Applications. *J. Bioelectron. Nanotechnol* **2016**, *1*, No. 9.

(14) Yurderi, M.; Bulut, A.; Ertas, İ. E.; Zahmakiran, M.; Kaya, M. Supported Copper−Copper Oxide Nanoparticles as Active, Stable and Low-Cost Catalyst in the Methanolysis of Ammonia−Borane for Chemical Hydrogen Storage. *Appl. Catal., B* **2015**, *165*, 169−175.

(15) Schwab, R. S.; Singh, D.; Alberto, E. E.; Piquini, P.; Rodrigues, O. E. D.; Braga, A. L. C−S Cross-Coupling of Thiols with Aryl Iodides under Ligand-Free Conditions Using Nano Copper Oxide as a Recyclable Catalyst in Ionic Liquid. *Catal. Sci. Technol.* **2011**, *1*, 569−573.

(16) Panova, Y. S.; Kashin, A. S.; Vorobev, M. G.; Degtyareva, E. S.; Ananikov, V. P. Nature of the Copper-Oxide-Mediated C−S Cross-Coupling Reaction: Leaching of Catalytically Active Species from the Metal Oxide Surface. *ACS Catal.* **2016**, *6*, 3637−3643.

(17) Wang, H.; Fan, W.; He, Y.; Wang, J.; Kondo, J. N.; Tatsumi, T. Selective Oxidation of Alcohols to Aldehydes/Ketones over Copper Oxide-Supported Gold Catalysts. *J. Catal.* **2013**, *299*, 10−19.

(18) Poreddy, R.; Engelbrekt, C.; Riisager, A. Copper Oxide as Efficient Catalyst for Oxidative Dehydrogenation of Alcohols with Air. *Catal. Sci. Technol.* **2015**, *5*, 2467−2477.

(19) Wang, S.; Gao, S.; Tian, J.; Wang, Q.; Wang, T.; Hao, X.; Cui, F. A Stable and Easily Prepared Copper Oxide Catalyst for Degradation of Organic Pollutants by Peroxymonosulfate Activation. *J. Hazard. Mater.* **2020**, *387*, No. 121995.

(20) Yang, M.; He, J. Fine Tuning of the Morphology of Copper Oxide Nanostructures and Their Application in Ambient Degradation of Methylene Blue. *J. Colloid Interface Sci.* **2011**, *355*, 15−22.

(21) Vargeese, A. A.; Muralidharan, K. Kinetics and Mechanism of Hydrothermally Prepared Copper Oxide Nanorod Catalyzed Decomposition of Ammonium Nitrate. *Appl. Catal., A* **2012**, *447−448*, 171−177.

(22) Karthikeyan, S.; Chuaicham, C.; Pawar, R. R.; Sasaki, K.; Li, W.; Lee, A. F.; Wilson, K. Template Free Mild Hydrothermal Synthesis of Core−Shell Cu_2O (Cu)@CuO Visible Light Photocatalysts for N-Acetyl-Para-Aminophenol Degradation. *J. Mater. Chem. A* **2019**, *7*, 20767−20777.

(23) Karthikeyan, S.; Kumar, S.; Durndell, L. J.; Isaacs, M. A.; Parlett, C. M. A.; Coulson, B.; Douthwaite, R. E.; Jiang, Z.; Wilson, K.; Lee, A. F. Size-dependent Visible Light Photocatalytic Performance of Cu_2O Nanocubes. *ChemCatChem* **2018**, *10*, 3554−3563.

(24) Karthikeyan, S.; Ahmed, K.; Osatiashtiani, A.; Lee, A. F.; Wilson, K.; Sasaki, K.; Coulson, B.; Swansborough-Aston, W.; Douthwaite, R. E.; Li, W. Pompon Dahlia-like Cu_2O/RGO Nanostructures for Visible Light Photocatalytic H2 Production and 4-chlorophenol Degradation. *ChemCatChem* **2020**, *12*, 1699−1709.

(25) Sekar, K.; Chuaicham, C.; Balijapalli, U.; Li, W.; Wilson, K.; Lee, A. F.; Sasaki, K. Surfactant-and Template-Free Hydrothermal Assembly of Cu_2O Visible Light Photocatalysts for Trimethoprim Degradation. *Appl. Catal., B* **2021**, *284*, No. 119741.

(26) Karthikeyan, S.; Dionysiou, D. D.; Lee, A. F.; Suvitha, S.; Maharaja, P.; Wilson, K.; Sekaran, G. Hydroxyl Radical Generation by Cactus-like Copper Oxide Nanoporous Carbon Catalysts for Microcystin-LR Environmental Remediation. *Catal. Sci. Technol.* **2016**, *6*, 530−544.

(27) Wang, S.; Liu, K.; Yao, X.; Jiang, L. Bioinspired Surfaces with Superwettability: New Insight on Theory, Design, and Applications. *Chem. Rev.* **2015**, *115*, 8230−8293.

(28) Sun, T.; Feng, L.; Gao, X.; Jiang, L. Bioinspired Surfaces with Special Wettability. *Acc. Chem. Res.* **2005**, *38*, 644−652.

(29) Sharma, V.; Orejon, D.; Takata, Y.; Krishnan, V.; Harish, S. *Gladiolus dalenii* Based Bioinspired Structured Surface via Soft Lithography and Its Application in Water Vapor Condensation and Fog Harvesting. *ACS Sustainable Chem. Eng.* **2018**, *6*, 6981−6993.

(30) Sharma, V.; Kumar, S.; Krishnan, V. Clustered Au on TiO_2 Snowman-Like Nanoassemblies for Photocatalytic Applications. *ChemistrySelect* **2016**, *1*, 2963−2970.

(31) Goldsmith, T. H.; Philpott, D. E. The Microstructure of the Compound Eyes of Insects. *J. Biophys. Biochem. Cytol.* **1957**, *3*, 429−440.

(32) Vértesy, Z.; Bálint, Z.; Kertész, K.; Vigneron, J. P.; Lousse, V.; Biró, L. P. Wing Scale Microstructures and Nanostructures in Butterflies−Natural Photonic Crystals. *J. Microsc.* **2006**, *224*, 108−110.

(33) Liu, K.; Du, J.; Wu, J.; Jiang, L. Superhydrophobic Gecko Feet with High Adhesive Forces towards Water and Their Bio-Inspired Materials. *Nanoscale* **2012**, *4*, 768−772.

(34) Sharma, V.; Balaji, R.; Kumar, A.; Kumari, N.; Krishnan, V. Bioinspired 3D Surface-Enhanced Raman Spectroscopy Substrates for Surface Plasmon Driven Photoxidation Reactions: Role of Catalyst and Substrate in Controlling the Selectivity of Product Formation. *ChemCatChem* **2018**, *10*, 975−979.

(35) Sharma, V.; Kumar, S.; Jaiswal, A.; Krishnan, V. Gold Deposited Plant Leaves for SERS: Role of Surface Morphology, Wettability and Deposition Technique in Determining the Enhancement Factor and Sensitivity of Detection. *ChemistrySelect* **2017**, *2*, 165−174.

(36) Sharma, V.; Balaji, R.; Krishnan, V. Fog-Harvesting Properties of *Dryopteris marginata*: Role of Interscalar Microchannels in Water-Channeling. *Biomimetics* **2018**, *3*, No. 7.

(37) Ikoma, T.; Kobayashi, H.; Tanaka, J.; Walsh, D.; Mann, S. Microstructure, Mechanical, and Biomimetic Properties of Fish Scales from *Pagrus major*. *J. Struct. Biol.* **2003**, *142*, 327−333.

(38) Liu, H.; Wang, Y.; Huang, J.; Chen, Z.; Chen, G.; Lai, Y. Bioinspired Surfaces with Superamphiphobic Properties: Concepts, Synthesis, and Applications. *Adv. Funct. Mater.* **2018**, *28*, No. 1707415.

(39) Kong, T.; Luo, G.; Zhao, Y.; Liu, Z. Bioinspired Super-wettability Micro/Nanoarchitectures: Fabrications and Applications. *Adv. Funct. Mater.* **2019**, *29*, No. 1808012.

(40) Sharma, V.; Koivikko, A.; Yiannacou, K.; Lahtonen, K.; Sariola, V. Flexible Biodegradable Transparent Heaters Based on Fractal-like Leaf Skeletons. *npj Flexible Electron.* **2020**, *4*, No. 27.

(41) Elsayes, A.; Sharma, V.; Yiannacou, K.; Koivikko, A.; Rasheed, A.; Sariola, V. Plant-based Biodegradable Capacitive Tactile Pressure Sensor Using Flexible and Transparent Leaf Skeletons as Electrodes and Flower Petal as Dielectric Layer. *Adv. Sustainable Syst.* **2020**, *4*, No. 2000056.

(42) Sharma, V.; Jääskö, K.; Yiannacou, K.; Koivikko, A.; Lampinen, V.; Sariola, V. Performance Comparison of Fast, Transparent and Biotic Heaters Based on Leaf Skeletons. *Adv. Eng. Mater.* **2022**, No. 2101625.

(43) Sharma, V.; Ali-Löytty, H.; Koivikko, A.; Yiannacou, K.; Lahtonen, K.; Sariola, V. Copper Oxide Microtufts on Natural Fractals for Efficient Water Harvesting. *Langmuir* **2021**, *37*, 3370−3381.

(44) Xu, L.; Xu, H.-Y.; Wang, F.; Zhang, F.-J.; Meng, Z.-D.; Zhao, W.; Oh, W.-C. Microwave-Assisted Synthesis of Flower-like and Plate-like CuO Nanopowder and Their Photocatalytic Activity for Polluted Lake Water. *J. Korean Ceram. Soc.* **2012**, *49*, 151−154.

(45) Mahmoud, A. E. D.; Al-Qahtani, K. M.; Alflaij, S. O.; Al-Qahtani, S. F.; Alsamhan, F. A. Green Copper Oxide Nanoparticles for Lead, Nickel, and Cadmium Removal from Contaminated Water. *Sci. Rep.* **2021**, *11*, No. 12547.

(46) Baylan, N.; İlalan, İ.; İnci, İ. Copper Oxide Nanoparticles as a Novel Adsorbent for Separation of Acrylic Acid from Aqueous Solution: Synthesis, Characterization, and Application. *Water, Air, Soil Pollut.* **2020**, *231*, 1−15.

(47) Sharma, V.; Yiannacou, K.; Karjalainen, M.; Lahtonen, K.; Valden, M.; Sariola, V. Large-Scale Efficient Water Harvesting Using Bioinspired Micro-Patterned Copper Oxide Nanoneedle Surfaces and Guided Droplet Transport. *Nanoscale Adv.* **2019**, *1*, 4025−4040.

(48) Koivikko, A.; Lampinen, V.; Yiannacou, K.; Sharma, V.; Sariola, V.Biodegradable, Flexible and Transparent Tactile Pressure Sensor Based on Rubber Leaf Skeletons. In *2020 IEEE Sensors*; IEEE, 2020; pp 1−4.

(49) Sharma, V.; Koivikko, A.; Yiannacou, K.; Lahtonen, K.; Sariola, V. Flexible Biodegradable Transparent Heaters Based on Fractal-like Leaf Skeletons. *npj Flexible Electron.* **2020**, *4*, No. 27.

(50) Sharma, V.; Yiannacou, K.; Karjalainen, M.; Lahtonen, K.; Valden, M.; Sariola, V. Large-Scale Efficient Water Harvesting Using Bioinspired Micro-Patterned Copper Oxide Nanoneedle Surfaces and Guided Droplet Transport. *Nanoscale Adv.* **2019**, *1*, 4025−4040.

(51) Mageshwari, K.; Sathyamoorthy, R. Physical Properties of Nanocrystalline CuO Thin Films Prepared by the SILAR Method. *Mater. Sci. Semicond. Process.* **2013**, *16*, 337−343.

(52) Wang, F.; Li, H.; Yuan, Z.; Sun, Y.; Chang, F.; Deng, H.; Xie, L.; Li, H. A Highly Sensitive Gas Sensor Based on CuO Nanoparticles Synthetized via a Sol−Gel Method. *RSC Adv.* **2016**, *6*, 79343−79349.

(53) Biesinger, M. C. Advanced Analysis of Copper X-ray Photoelectron Spectra. *Surf. Interface Anal.* **2017**, *49*, 1325−1334.

(54) Cudennec, Y.; Lecerf, A. The Transformation of $Cu(OH)_2$ into CuO, Revisited. *Solid State Sci.* **2003**, *5*, 1471−1474.

(55) Rioux, R. M.; Vannice, M. A. Hydrogenation/Dehydrogenation Reactions: Isopropanol Dehydrogenation over Copper Catalysts. *J. Catal.* **2003**, *216*, 362−376.

(56) Santacesaria, E.; Carotenuto, G.; Tesser, R.; Di Serio, M. Ethanol Dehydrogenation to Ethyl Acetate by Using Copper and Copper Chromite Catalysts. *Chem. Eng. J.* **2012**, *179*, 209−220.

(57) Astruc, D.; Lu, F.; Aranzaes, J. R. Nanoparticles as Recyclable Catalysts: The Frontier between Homogeneous and Heterogeneous Catalysis. *Angew. Chem., Int. Ed.* **2005**, *44*, 7852−7872.

(58) Kondo, K.; Akolkar, R. N.; Barkey, D. P.; Yokoi, M. *Copper Electrodeposition for Nanofabrication of Electronics Devices*, Springer, 2014; Vol. *171*.

(59) Hirsimäki, M.; Lampimäki, M.; Lahtonen, K.; Chorkendorff, I.; Valden, M. Investigation of the Role of Oxygen Induced Segregation of Cu during Cu2O Formation on Cu {1 0 0}, Ag/Cu {1 0 0} and Cu (Ag) Alloy. *Surf. Sci.* **2005**, *583*, 157−165.